Optimizing Stub-to-Carbon Contact for Higher Amperage in Aluminium Smelting – A Computational Study

Tushar Thorat[1], Dibyendu Ghosh[2], Devendra Pathe[3], Venkannababu Thalagani[4] and Amit Gupta[5]
1,4. Senior Scientist
5. Senior Lead Scientist
Aditya Birla Science & Technology Company, Navi Mumbai, India.
2. Manager, Carbon Plant
3. Assistant General Manager, Pot-room
Hindalco Mahan, Singrouli, India
Corresponding author: tushar.thorat@adityabirla.com
https://doi.org/10.71659/icsoba2025-el018

Abstract

With the rising demand for aluminum, many manufacturers are expanding their production capacity through greenfield and brownfield expansions, as well as by increasing amperage in existing potlines. Among these, amperage increase has emerged as the most popular option due to its ability to deliver higher productivity gains with relatively lower investment. Modern pots are designed to operate at specific amperage levels. To achieve higher amperage while maintaining thermal balance and similar direct current energy input, key design modifications are necessary. Published literature identifies cathode lining and anode design adjustments as critical changes required for such upgrades. In this study, we developed an FEA-based computational model to predict the stub-to-carbon contact voltage drop. The model was validated through plant measurements. This paper further presents a parametric study evaluating the impact of amperage increase on stub-to-carbon contact drop. Additionally, various stub hole design modifications were simulated to identify solutions for reducing voltage drop without compromising the mechanical strength of the stub-to-carbon connection.

Keywords: Aluminium Smelting, Amperage increase, Stub to Carbon Drop, Stub hole design

1. Introduction

Mahan Aluminium has an AP 36 potline designed for 360 kA. In the recent past, smelter have raised the amperage to 376 kA to meet the increased demand for aluminum. This increase in amperage has led to a rise in anode current density from 0.893 A/cm^2 to 0.917 A/cm^2. To fully leverage the potential of amperage ramp-up, the smelter is planning to further increase it to 400 kA. Raising amperage also impact the voltage drop across the potline. The pot process control logic operates based on a set pot voltage value. An increase in ohmic drop, caused by a higher voltage drop in the anode assembly, is ideally offset by reducing the interpolar distance or the distance between the anode and cathode. However, decreasing the interpolar distance makes the pot more susceptible to MHD (magnetohydrodynamics) instabilities. In order to keep the interpolar distance constant, it is necessary to adjust the pot's set voltage value. This adjustment results in higher specific DC (Direct Current) energy consumption. Design modifications in the anode assembly and cathode lining offer an opportunity to decrease the ohmic drop across the pot and run the smelter with lower specific energy, even at higher amperage. Previous studies have reported such efforts in amperage increase campaigns [1]. In this paper, prime focus is on anode assembly design. Anode assembly voltage drop is divided into various components such as rod drop, bimetallic or transition joint drop, yoke drop, stub to carbon drop and anode block drop. Stub to carbon contact drop in anode assembly accounts for ~30 % of total anode voltage drop. The magnitude of electrical resistance across the contact surface between the anode block and the

cast-iron thimble depends on the surface roughness and the effective contact pressure generated on the contact surface. The intensity/magnitude of the contact pressure depends on the initial air gap between the cast iron and the stub hole, as well as the thermal expansion of the cast iron thimble and stub during the process in the pot. In addition to the pouring temperature of the liquid cast iron and the preheating temperature of the carbon block and pin, the geometry of the stub hole and the thickness of the cast iron also play important roles in determining the value of the initial air gap. Optimization of the stub-to-carbon contact has been a topic of interest for the aluminum smelting community for a long time. Many experimental and computational studies have been conducted in the past to improve the stub hole design and pin design to reduce the drop of the stub to carbon contact [2–4].

In this paper, a FEA (Finite Element Analysis)-based computational model is developed to examine the impact of stub hole design modifications on the thermal, electrical, and mechanical behavior of the anode assembly. This model is utilized to conduct simulations and analysis to optimize the stub hole design and transition joint to reduce the ohmic drop across the anode assembly.

2. Computational Model Development

This section describes the anode assembly geometry, meshing details, boundary conditions and analysis procedure used in the model.

2.1 Geometry

Each anode assembly consists of one anode rod, one hexapod, a transition joint, six cast iron thimbles, and two carbon anode blocks. The distance between two anode blocks is 10 mm. To reduce simulation time, only half of the anode assembly is modelled.

3D geometry used in the model is shown in Figure 1. It includes (i) half anode assembly comprising half anode rod, half transition joint, half hexapod, pins, three cast iron thimbles, and one anode block. According to operational practice, stub to carbon drop measurements is conducted after 5–6 days of installation of the anode block. Historically measured data forms the basis for analyzing the impact of operating conditions on the anode assembly voltage drop. Therefore, the anode block height at half-life is considered in the geometry.

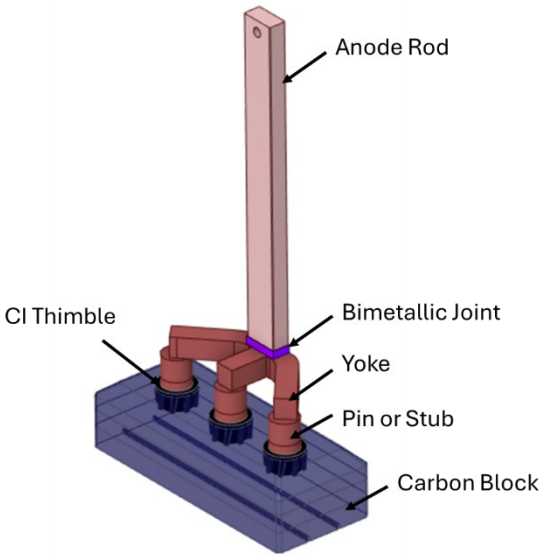

Figure 1. Anode assembly geometry considered as modeling domain.

2.2 Meshing Details and Material Properties

The model in this study is designed for fully coupled thermal-electric-mechanical analysis using the ANSYS commercial code version 2022R2. Elements were chosen based on their shape and degrees of freedom. The Solid 227 element, a tetrahedral element with 10 nodes, was utilized to create a mesh for solid parts in the geometry. Each node has up to six degrees of freedom to solve coupled thermal-electric-mechanical physics. The model consists of eight contact pairs, with CONTA174 and TARGE170 elements used to create mesh in contact and target surfaces, respectively. These elements allow for the imposition of translational or rotational displacement, temperature, voltage, magnetic potential, forces, moments, and pore pressure on the target segment element. Contact element sizing was assigned to each contact pair based on the complexity of the surface geometry. Additionally, the mesh includes surface elements to transfer thermal, electrical, and structural loads to the underlying solid elements. SURF152 was applied for thermal and electrical loads, while SURF154 was used for structural loads [5]. To optimize simulation time and capture detailed behavior in critical regions, the mesh density was varied. A finer mesh was generated around contact interfaces and components with small edges, curves, and areas, such as cast-iron thimbles. Details of element type and mesh count are provided in Table 1. Figure 2 shows the visual presentation of the mesh used in the model.

Temperature dependent property data sets were provided for thermal coefficient of expansion, thermal conductivity, and electrical conductivity. However, constant values were used for defining density, yield strength, modulus of elasticity and Poisson's ratio.

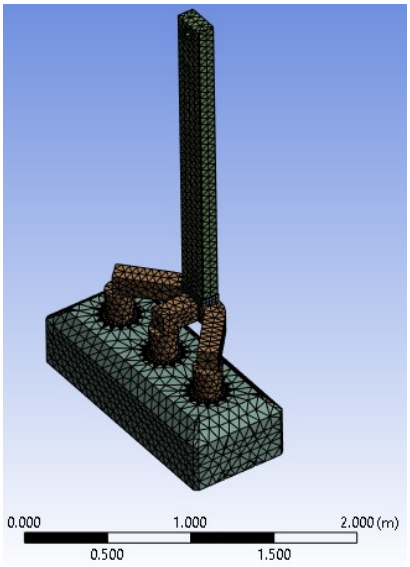

Figure 2. Visual presentation of the mesh used in the model.

Table 1 Details of element type and mesh count.

Component	Element Type	Edge length (mm)	Element Count
Anode Rod	SOLID 227	50	73877
Transition Joint	SOLID 227	25	
Hexapod	SOLID 227	50	
Cast iron thimble	SOLID 227	25	
Carbon Block	SOLID 227	75	
Contact Pairs	CONTA174 and TARGE170	10	66214
Total			126671

2.3 Boundary conditions and analysis settings

The model presented in this study assumes that an anode assembly is placed in an operating pot and subjected to the corresponding ambient conditions. The boundary conditions applied can be categorized into three main areas: (i) Electrical boundary conditions, (ii) Thermal boundary conditions, and (iii) Structural boundary conditions.

2.3.1 Electrical Boundary Conditions

In the base case, it is assumed that the pot is operating at a current of 360 kA. Each pot has 20 anode assemblies, with each assembly containing two carbon anode blocks. As mentioned before, only half of the anode assembly is considered in the computational domain. Therefore, a current of 9 kA is input from the anode beam-anode rod connection. The area of the carbon anode block immersed in the bath is given a ground voltage boundary condition. A visual representation is shown in Figure 3.

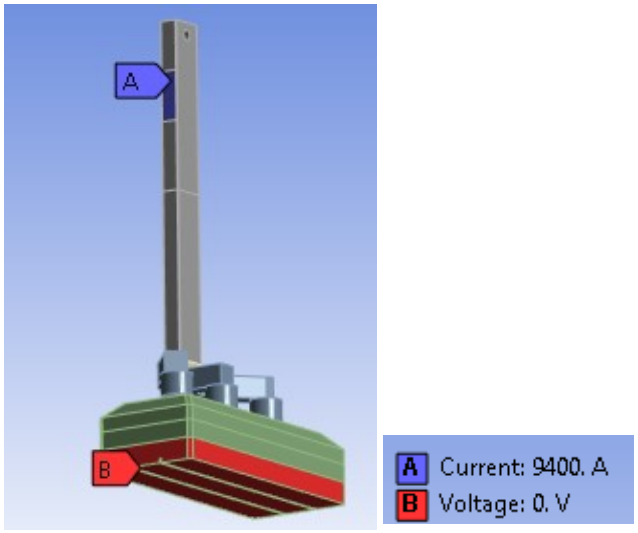

Figure 3. Electrical boundary conditions applied in base case.

2.3.2 Thermal Boundary Conditions

In the typical installation setup, the hexapod, pins, and some parts of the anode rod are exposed to the hot fumes emanating from the pot. Part of the anode block is submerged in the bath, some is exposed to radiation from the crust and liquid bath, and the remaining part is covered by a mixture of bath and alumina (referred to as the anode cover). The surface of the anode cover is also exposed to the hot gases under the hood covers. Due to varying surrounding conditions, different convective and radiative boundary conditions were applied to different surfaces of the anode assembly geometry. Convective heat transfer coefficients were calculated based on temperature, and ambient temperature values were determined according to the average temperatures experienced in different areas. Thermal emissivity values were assigned to surfaces where radiation played a significant role in heat transfer. Figure 4 shows the visual presentation of various surfaces used as thermal boundaries. The detailed description of boundary conditions can be found in Table 2.

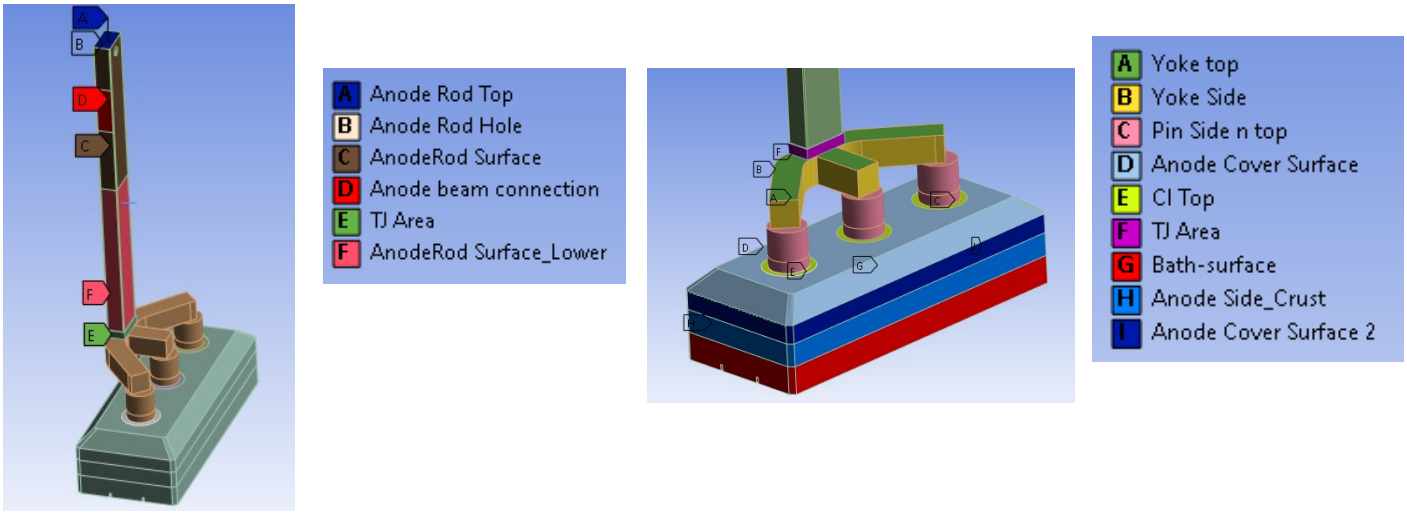

Figure 4. Visual presentation of various surfaces used as thermal boundaries.

Table 2. Description of thermal boundary conditions.

Area	Boundary Condition	Ambient Temp (ºC)	Heat Transfer Coefficient	Thermal Emissivity
Anode Rod Top	Convection	40	Temperature Dependent HTC Data	NA
Anode Rod Hole		40		
Anode Rod Surface	Convection and Radiation	40		0.8
Anode Rod Surface Lower		130		0.8
Anode Beam Connection	Temperature	90		
TJ Area	Convection	130		
Yoke top, Yoke Side	Convection and Radiation	130		0.8
Pin Side and Top		150		0.8
Anode Top Surface		180		0.9
CI thimble Top Surface		180		0.9
Anode Side Crust		750		0.9
Bath Surface	Convection	960	5000	

2.3.3 Structural Boundary Conditions

Support was fixed at the connecting area between the anode beam and anode rod. A positive gravitational acceleration was applied to accommodate the suspended load of the anode assembly.

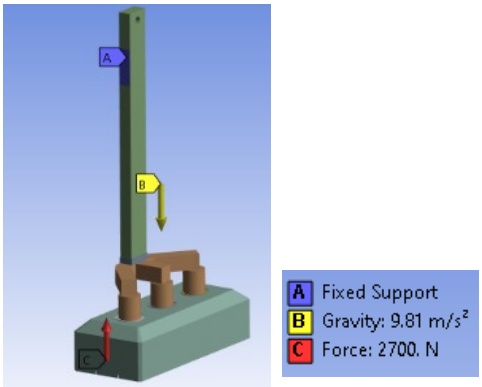

Figure 4. Structural boundary conditions applied in model.

Additionally, a force was applied to the bottom surface of the anode block to account for the buoyancy forces caused by the immersion of the anode block in the bath.

2.3.4 Contact Pair Settings

In a typical anode assembly, anode rods, bimetallic joint and hexapod are welded together. These connections are represented as bonded contacts. Electrical conductance values across contacts were adjusted to obtain the realistic value of voltage drops.
During the rodding phase cast iron normally shrinks onto the steel pins. This phenomenon creates an almost perfect contact between pin and cast-iron thimble. Therefore, these pairs are also treated as bonded contact and a suitable electrical contact conductance value was provided to obtain realistic voltage drop.
Due to shrinkage of cast iron during its solidification, a very small (few hundred microns) air gap is created between cast iron and carbon block's stub hole during rodding phase. Current distribution measurements across different age anode assemblies show that after 3–4 days of anode assembly installation cast iron expands to exert sufficient contact pressure to reduce the contact voltage drop. In present study it is assumed that the anode assembly is 9 days old. Hence, no initial gap was provided between cast iron thimble and stub hole. Cast iron-carbon contact pairs were treated as frictional contacts. Value of coefficient of friction was adopted from K. Ding's work [6]. The contact stiffness factor was updated to ensure accurate penetration and contact pressure calculations. A subroutine for defining electrical conductance as a function of contact pressure was developed and incorporated into the model. The contact pressure vs. contact resistance data was adopted from D. Richard's work [7].

3. Results

3.1 Model Validation

Plant measurements were performed to gather the data for voltage drop and temperature at various locations in anode assembly. 5 anode assemblies, 9-day old, were selected for these measurements. Figure 4 shows the locations of the probes during the measurement.

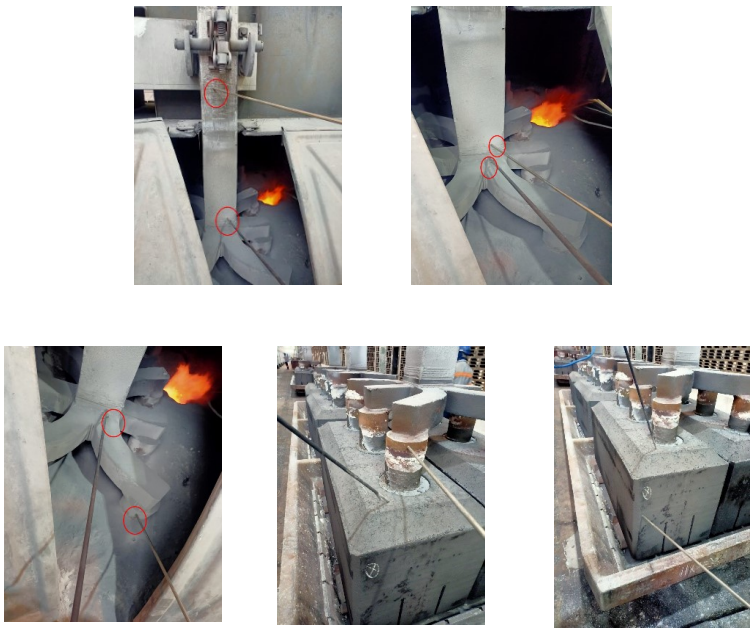

Figure 4. Locations of the probes during the anode assembly voltage measurement.

Thermal imaging technique was used to measure the temperature of yoke, pin and bimetallic joint. Computed thermal profile was compared against this data for validation purpose. Voltage drop and thermal profile across anode assemblies are shown in Figure 5. Comparison of computed and measured voltage drop is shown in Table 3. Computed thermal and electrical results were found in good agreement with measured data. However, a deviation in measured and computed voltage drop was observed for the 'hexapod to pin' region. Higher measured values can be linked to variation in readings due to yoke-pin weld joint quality, pin dimensions and presence of anode cover coating on the pin surface.

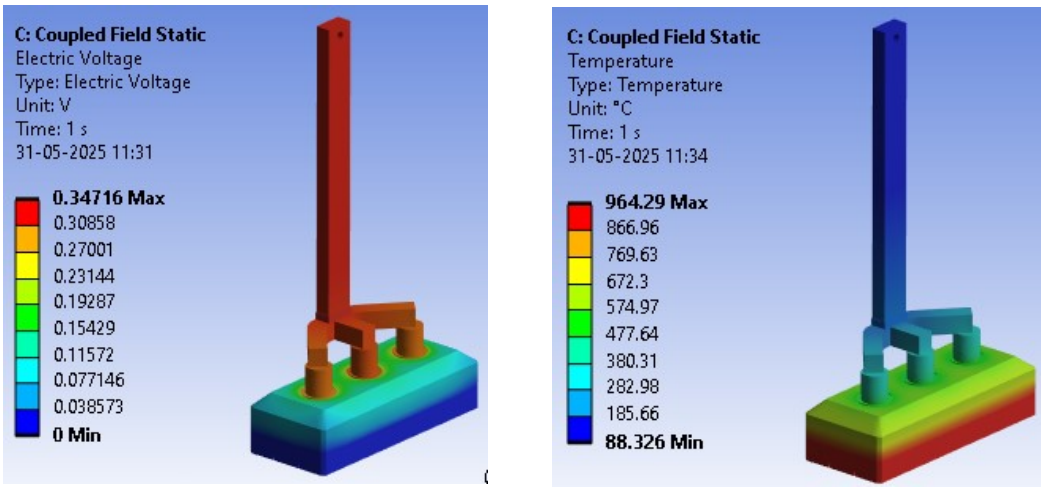

Figure 5. (a) Voltage drop (V) across anode assembly (b) thermal profile across anode assembly.

Table 3. Comparison of measured and computed voltage drop.

Component	Measured, mV	Computed, mV
Anode Rod	24	22
Transition Joint	6	5
Hexapod and Pin	39	32
Stub to Carbon	106	107
Carbon Block	176	178

Contact pressure profile and current density distribution across CI-Carbon joint is shown in Figure 6. As indicated, maximum contact pressure was observed across the flutes of the cast iron thimble. Current density magnitude was observed to directly related to the contact pressure.

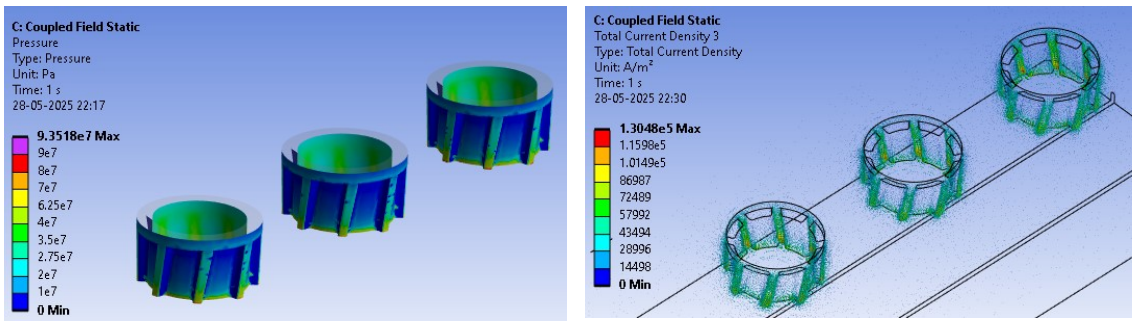

Figure 6. (a) Contact pressure across pin-CI and CI-carbon connections (b) Current density distribution across CI-carbon connection.

3.2 Parametric Analysis

Different design options were tested with the objective of (i) analysing the impact of amperage increase on voltage drop across existing anode assembly and (ii) reducing the voltage drop at high amperage operation. The scheme of simulation is summarized in the next Table 4.

Table 4. Scheme of simulation used in parametric analysis.

Parameter	Base Case	Case 1	Case 2	Case 3
Pin Diameter (mm)	180	180	190	190
Stub Hole Depth (mm)	130	130	130	145
Amperage (kA)	376	390	390	390
Anode Length (mm)	1580	1580	1580	1610

Case 1 was simulated to analyze the impact of amperage increase on voltage drop, thermal profile and mechanical stresses across the existing anode assembly. In case 2, the pin diameter was increased by 10mm. Anode block design and amperage were kept constant as that of case 1. In case 3, the stub hole depth was increased by 15 mm. This modification led to increased height of cast iron thimble and length of helical flutes. At the same time anode length was increased by 30 mm. Comparative analysis of voltage drop across different components in anode assembly for these three cases is provided in Table 5.

Table 5. Voltage drop across different components in anode assembly for cases 1, 2 and 3.

Component of voltage drop, mV	Base Case	Case 1	Case 2	Case 3
Anode Rod	24	25	25	25
Transition Joint	6	7	7	7
Hexapod to Pin	32	34	34	34
Stub to Carbon	107	112	107	100
Carbon Block	178	184	185	175
Total	347	359	353	341

Comparative analysis shows that the voltage drop across anode assembly increases almost linearly with increase in amperage. Increasing pin diameter reduces cast iron thickness and increases cast iron pressure. Cumulative impact of these changes results in reduction in stub to carbon contact drop by ~5 mV. Increasing stub-hole depth provides more contact area which further provides additional ~7 mV saving in voltage drop. Increase in anode length by 30 mm reduces the current density which reduces the voltage drop across carbon anode block by ~10 mV.

4. Conclusion

Amperage creep in aluminium smelters leads to the increased ohmic drop in pot. To nullify the impact, it is necessary to modify the anode assembly and cathode lining design. A computational model was developed and validated for analysing impact of amperage increase and design modification in anode assembly. Parametric analysis was performed to understand impact of amperage increase, stub hole design modification, pin design modification and anode block design modification on thermal and electrical performance of anode assembly. It was observed that anode assembly voltage drop increases almost linearly with the amperage increase. Increase pin diameter and stub-hole depth can assist in reducing stub to carbon drop. Increasing stub hole depth is a more effective option. To reduce the drop across the anode block, it is necessary to increase overall cross section to reduce anode current density.

5. References

1. M.A. Shukralla, et al., The roadmap of AP-ALBA to 400 kA, *Proceedings of 39th International ICSOBA Conference, Virtual Conference,* 22 – 24 November 2021, *TRAVAUX* 50, 625–635.
2. D.R. Gunasegaram, D. Molenaar, Towards improved energy efficiency in the electrical connections of Hall Heroult cells through finite element analysis (FEA) modeling, *Journal of Cleaner Production*, 2015, 1–19.
3. D. Molenaar, et al., Experimental investigation of factors affecting the electrical performance of the stub to carbon connection, *Light Metals* 2013, 1359–1364.
4. D.A. Sinaga et al., Stub to carbon design improvement, *Proceedings of 41st International ICSOBA Conference,* Dubai, UAE, 5 – 9 November 2023, *TRAVAUX* 52, 1007–1016.
5. ANSYS, ANSYS Mechanical APDL Element Reference, 2014.
6. K. Ding, et al., Prediction of voltage loss on electrical connections for aluminium smelter reduction cells, *Proceedings of the Institution of Mechanical Engineers*, Part C: Journal of Mechanical Engineering Science, 2012, 981–994.
7. D. Richard, et al., Carbon to cast iron electrical contact resistance constitutive model for finite element analysis, *Journal of Materials Processing Technology*, 132, 2003, 119–131.